VOL. 76, NO. 14 JOURNAL OF GEOPHYSICAL RESEARCH MAY 10, 1971

An Analysis of Marvel—A Nuclear Shock-Tube Experiment

BARBARA K. CROWLEY, H. DAVID GLENN, AND ROBERT E. MARKS

Lawrence Radiation Laboratory
University of California, Livermore 94550

Marvel, a nuclear-driven shock-tube experiment, consisted of a 2.2-kT nuclear explosive detonated 176 meters underground at one end of a 122-meter long, 1-meter diameter horizontal tunnel. Vaporization of material in the immediate vicinity of the explosive provided the source of high-energy driven gas. The driven gas was the ambient atmospheric air in the tunnel. Marvel was conducted as an experimental and calculational study of the time-dependent flow of energy in the tunnel and surrounding alluvium. This paper describes (1) the design of Marvel, (2) the dynamic and postshot experimental results, and (3) a numerical simulation of the experiment. Experimental and calculational results indicate the following. The high-energy air shock traveled down the tunnel nearly 50 times faster than the shock in the surrounding alluvium. Over the first 30 meters of the tunnel, the shock had a velocity of approximately Mach 380; during its 4-msec transit of the 122-meter tunnel, it attenuated to approximately Mach 30. Significant ablation of material from the tunnel walls had the primary effect in attenuating the air shock. The source energy was preferentially channeled down the tunnel, and a cone-shaped cavity resulted.

Marvel, a nuclear shock-tube experiment, consisted of an air-filled, horizontal tunnel 1 meter in diameter and 122 meters long, at a depth of 176 meters below the surface. A 2.2-kT nuclear energy source was located at one end of this tunnel. The Marvel experiment was directed by the Lawrence Radiation Laboratory and conducted at the Atomic Energy Commission testing facility near Mercury, Nevada.

We have developed experimental and calculational experience with nuclear energy sources that were placed in nearly spherically symmetric initial geometries. These sources have been located at specific depths to produce either cavities [*Rodean,* 1968; *Butkovich,* 1965; *Rogers,* 1966] or craters [*Cherry,* 1967] in various geological media. Marvel was located well below cratering depth in alluvium. The purpose of Marvel was to develop improved experimental and calculational capabilities for understanding the propagation of energy in a nonspherical initial geometry.

Before Marvel, it was not known whether a nonspherical initial geometry would result in significant nonspherical energy deposition. If the energy deposition were sufficiently nonspherical, the pattern and intensity of the outgoing shock, the cracked regions, and the final cavity shape would also be nonspherical. Thus, by suitable design of the initial emplacement configuration, it might be possible to produce cavities and cracked regions in other than spherical shapes. For instance, the deposition of nuclear energy could be tailored to local geological conditions for mining, gas stimulation, and other applications [*Rodean,* 1968; *Butkovich,* 1965].

Marvel was an initial Plowshare effort in nonspherical source studies. Consequently, the development of new experimental techniques was required to monitor the exotic range of gas-dynamic flow variables encountered.

If the surrounding medium is not severely layered, an experiment can be simulated numerically by one-dimensional calculations until the shock reaches the surface. However, the one-dimensional approach is not adequate for nonspherical experiments. The flow of high-energy gas from the source region and the propagation of the shock wave into the surrounding solid medium are two very different types of flow. To simulate these two flows, a calculation was developed that simultaneously considers the basic physics of high-energy gas dynamics and of rock mechanics.

A dominant feature of Marvel was the combining of ideas from both the calculational and experimental disciplines throughout the experiment. For instance, in the design and construction of Marvel, great care was taken to achieve an 'ideal calculable shock tube,' that is, a smooth tunnel surrounded by homogeneous media (alluvium) with a minimum of discontinuities. This was done in order to minimize the assumptions required for numerical simulation of the experiment.

In addition to the design and construction of Marvel and the dynamic and postshot experimental results, this paper describes the numerical codes, the initial conditions for the calculations, and the results of the calculations.

1. GENERAL DESIGN AND CONSTRUCTION OF THE EXPERIMENT

The original excavation for Marvel consisted of a vertical access shaft 1.2 meters in diameter, which terminated at a depth of 176 meters below the surface in a working room with dimensions approximately 6 × 4 × 4.5 meters high (see Figure 1). Later, the nuclear energy source was placed in this room at a position designated as the 'working point' in Figure 1. A main drift with a cross section of 1.5 × 2.1 meters was excavated horizontally for approximately 122 meters from the working point. Four alcoves, each 6 meters long and 1.5 × 2.1 meters in cross section, were excavated at right angles to and off the main drift. The centers of these alcoves were located at distances of approximately 30, 61, 83, and 102 meters from the working point. At the end of the main drift, a fifth slightly larger alcove was located in line of sight with the working point. The fifth alcove was used for early-time luminosity measurements. The results of these measurements have been reported [*Glenn and Crowley*, 1970].

Vertical cased holes for instrumentation cables were drilled from the surface to the back of each alcove. When instrumentation of the alcoves was completed, the alcoves and vertical cable holes were solidly backfilled with a grout that closely matched the density of the surrounding alluvium ($\sim$1.7 g/cm^3). After backfilling, only a volume of approximately 10 m^3 in the end of the fifth alcove remained, which permitted access by personnel at a later time.

To construct the final tunnel, 0.45-meter sec-

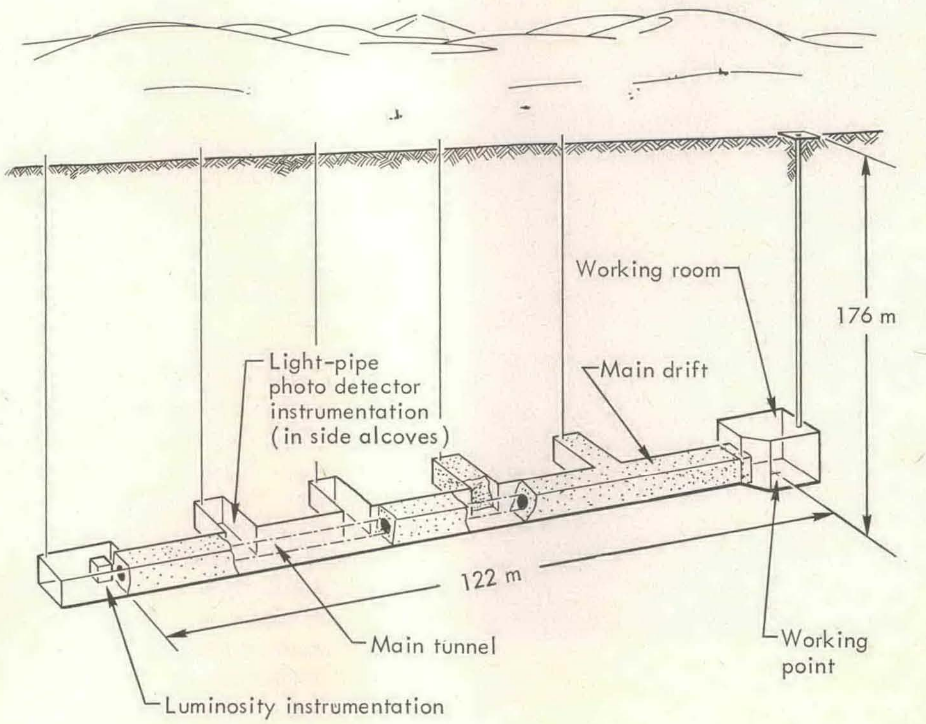

Fig. 1. General design of the Marvel experiment.

tions of circular Transite pipe (1.0 meter i.d., 1.07 meters o.d.) were placed along the 122-meter drift (Figure 2). In addition, five wall sections containing chemical tracers were located at specific distances from the working point. Details of these tracer sections and their use in obtaining ablation information are discussed in the next section. All the Transite and tracer sections were carefully joined with epoxy cement. A final examination of the 245 Transite and tracer sections in the assembled 122-meter tube showed an average offset in the joining of the sections of less than 0.3 cm. The remaining portion of the drift outside the Transite tunnel was then completely backfilled with the density-matching grout.

The energy source was placed in a specially designed cylindrical canister, 1.0 meter in diameter and 1.5 meters long. This canister was so designed that when the shock left the canister (1) the energy source would be homogeneous (i.e., the pressure would be nearly the same throughout the canister); (2) the shock down the tunnel would be a plane hydrodynamic shock (i.e., the emerging shock would span the diameter of the canister); and (3) the initial shock starting into the alluvium from the working point would be cylindrical. These requirements on canister design were made in order that the assumptions required to model the energy source region numerically would be minimized. The canister design was achieved by studying the effects of the arrangement of various materials within the canister on numerical calculations (L. A. Rogers, private communication, 1968; G. Pelsor, private communication, 1967).

After installation of the nuclear energy source, the working room was completely sandbagged. The main access shaft was then stemmed with gravel.

Thus, considering practical limitations (see Figure 2), great care was taken to achieve an 'ideal-calculable-shock-tube' design with a homogeneous source and no significant discontinuities in either the final tunnel or the surroundings. As discussed in Section 3, this design is readily adaptable to numerical modeling.

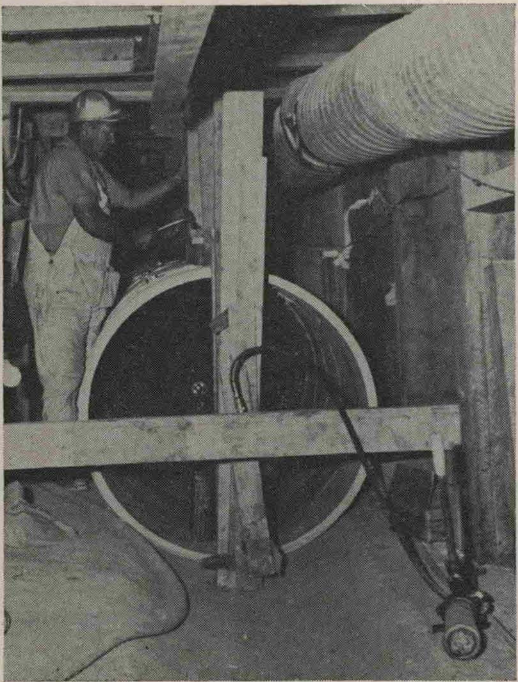

Fig. 2. Installation of the Transite pipe in the main drift. The concrete trough was first poured and cast to facilitate proper alignment of the Transite pipe sections.

2. Experimental Measurements

Dynamic Measurements

Instrumentation for obtaining dynamic data was installed along the 122-meter tunnel as well as in the alluvium above the detonation. The tunnel instruments included: (1) light-pipe photodetector systems [*Glenn and Crowley,* 1970] and tourmaline crystal gages; (2) slifers [*Heusinkveld and Holzer,* 1964] along the tunnel as well as perpendicular to the tunnel into the four alcoves; (3) stress-history gages in each of the four alcoves; and (4) specially designed cavity gas-pressure instrumentation at a position 100 meters from the device. The free-field alluvium instruments included slifers and stress gages placed in a vertical instrument hole parallel to the access shaft and 9.8 meters from the working point. Figure 3 shows the relative positions of the instrumentation used to measure the dynamics of the shock.

Air-shock time-of-arrival detection at the four alcoves. The time of arrival (TOA) of the air shock down the tunnel was determined at each of the four alcoves with a light-pipe photodetector system. A tourmaline crystal gage was mounted adjacent to these optical systems in

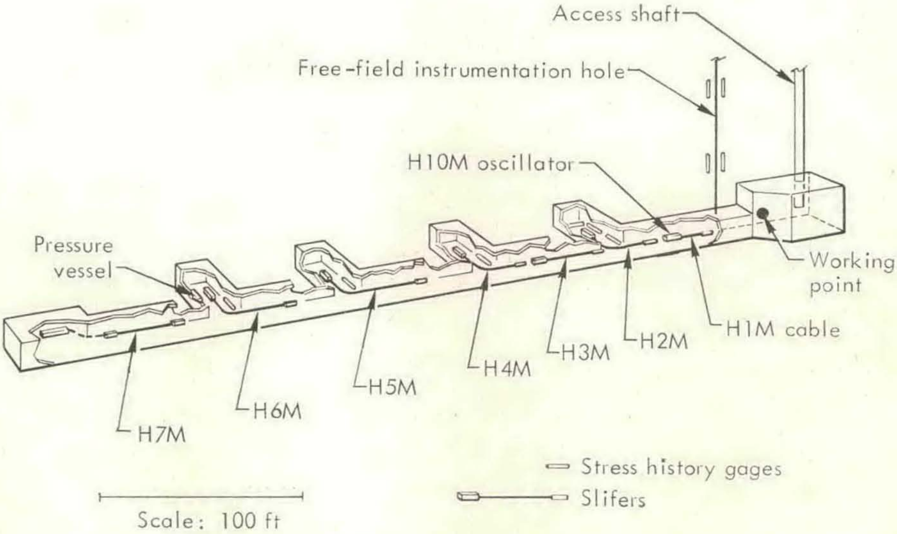

Fig. 3. Location of the slifers and stress-history gages.

the first and third alcoves to provide independent TOA checks. Figure 4 presents the results for these measurements; details have been reported by *Glenn and Crowley* [1970].

Slifers. Seven slifers were used to measure shock arrival in the tunnel and alcoves, and all produced useful data. Each slifer sensing cable was 12.2 meters long. The cables along the sides of the tunnel were buried 5 to 12 cm from the inside surface of the tunnel. The cables were wrapped with lead foil to inhibit radiation-induced ionization of the cable ahead of the shock wave.

Cavity gas-pressure instrumentation. In alcove no. 4 (100 meters from the device) a pressure-measuring system was installed (in a surplus 16-inch naval gun barrel). There was a silicone oil coupling between the tunnel and the pressure gages. The purpose of this system was to measure the late-time pressure in the cavity and tunnel (up to a few minutes after the shock had passed). The fluid coupling protects the pressure gages from the hot, radioactive gases. Two 100-kpsi-range gages and one 15-kpsi-range gage were used in the system. The 15-kpsi gage was located behind an orifice system designed to cut off the peak of the initial shock pulse and prevent overranging of the gage. This gage was to record the low pressure in the cavity after the initial shock wave. It was hoped that the very heavy hardware would protect the electronics and signal cables through the shock wave, but the system failed at about 17 msec, presumably from ground motion that resulted in severed signal cables. The 100-kpsi variable-reluctance pressure gage went into 'resonant saturation' with the onset of pressure. The 100-kpsi, bridge-type pressure gage performed well and recorded the signal shown in Figure 5. The 15-kpsi bridge gage gave little information because it was behind an orifice whose mechanical time constant was 3 msec. These pressure data are also given in Table 2, section 3, where a comparison with the calculations is made.

Free-field measurements. Two slifers were placed in the instrument hole that intersected the tunnel at 9.8 meters from the device. Both of these slifers gave good results. In addition, four piezoelectric stress gages were placed in two locations in this instrument hole (see Figure 3). These free-field data are also presented in section 3, where a comparison with the calculations is made.

To determine the position of the shock wave in the tunnel from the slifer closure, two corrections were made, one for the travel time of the shock from the tunnel to the cable, and another for the time it takes the cable to collapse after impact of the shock wave. Four of the slifers were placed with part of the cable along the tunnel and part of the cable turning the corner into the alcoves, where the cable was perpendicular to the tunnel. Agreement of the TOA data for the slifers, piezoelectric gages, and light-pipe photodetector system is illustrated in Figure 4.

The segments of the slifers located in the alcoves provided TOA data of the radial shock front in the grouted alcoves. These data are presented in Figure 6.

Stress history measurements. Six piezoelectric stress gages were placed in the four alcoves. There were three gages in the first alcove; two of these were oriented radially to the tunnel, and the third (in the back of the alcove) was radial to the device. The other three alcoves each contained a gage oriented radially to the tunnel and at a distance of 1 meter from the center line of the tunnel. All alcoves were filled in with alluvium-matching grout. Figure 3 also indicates the locations of the stress gages. The TOA data from the gages are given in Figure 6. Many of the gages recorded multiple shock pulses, but

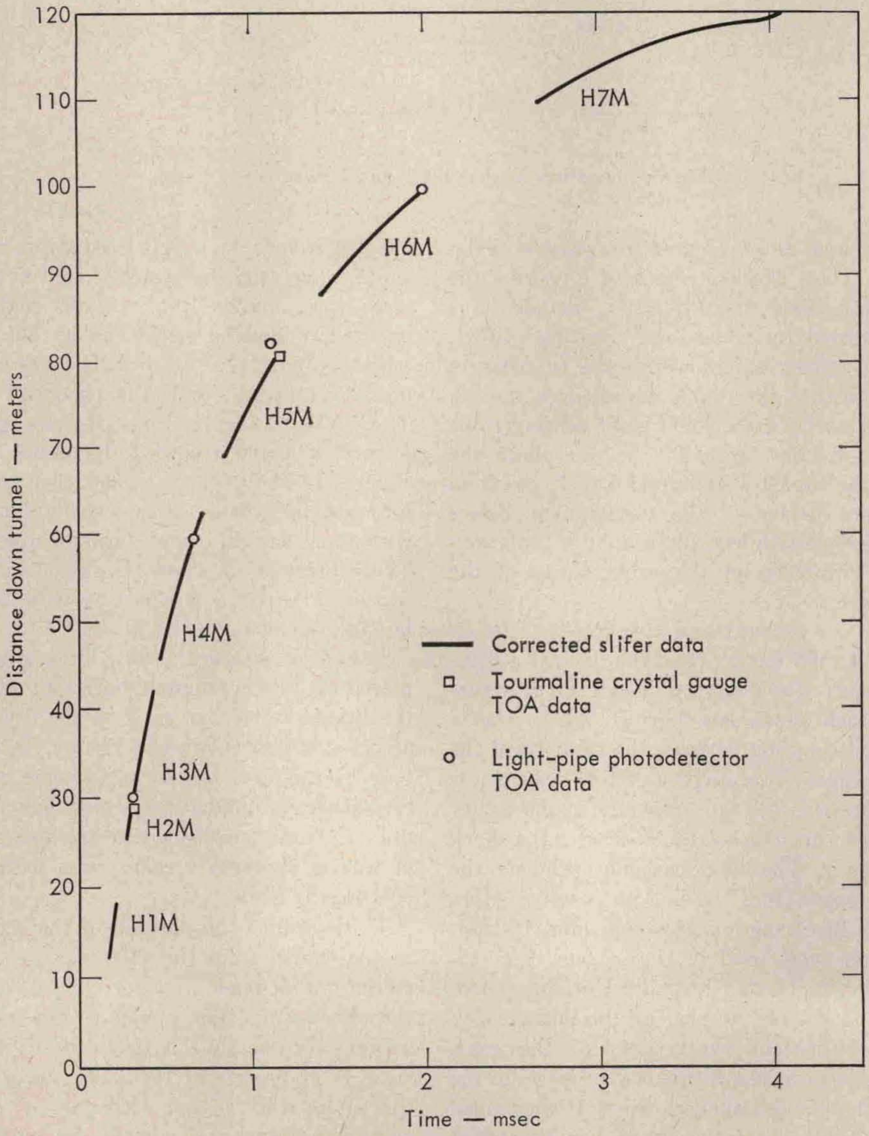

Fig. 4. TOA data of the shock front in the tunnel.

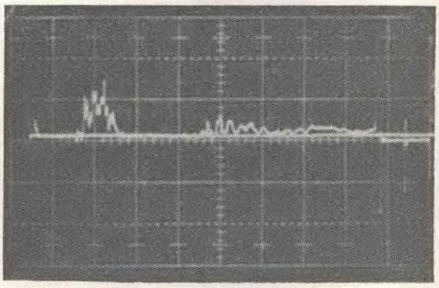

Fig. 5. Cavity gas-pressure instrumentation gage signal from alcove 4: 100-kpsi-range Norwood gage, 2 msec/cm, 25 kpsi/cm.

Figure 6 shows only the initial pulses. Further details of these stress-gage measurements are given in Table 2 in section 3, where a comparison with the calculations is made.

Postshot Measurements

Chemical tracer distribution. Five chemical tracer sections were fabricated and mounted at different locations along the tunnel to determine the quantity of wall material ablated by the passage of the shock wave and flow behind the shock. Each section was a 1-meter i.d., 6.1-meter long laminated right circular cylinder composed of two separate concentric layers containing different tracers. The thickness and quantity of tracers in each layer varied with location along the tunnel. The tracers were commercial-grade chemicals mixed with cement to form a loaded grout or concrete. Figure 7 and Table 1 show the locations of each section, thickness of the layers, and different tracers used. The inner layer for each section was the tunnel wall. Consequently, ablation of the inner layer had to occur before ablation of the outer layer could begin.

Mass spectrometer analyses of the postshot drill samples are shown in Figure 7 for the first three sections (L. A. Rogers, private communication, 1968). Tracers from these sections were distributed all along the tunnel, with the highest concentration at the 90- to 100-meter position. This position corresponds to the stagnation location of the flow discussed later. Results for the last two sections (not shown) indicated that only a small quantity of the inner layer was ablated.

Cavity formation and the subsidence crater. Chemical analyses of refractories from postshot drill cores suggested a significant nonspherical shape for the final cavity geometry just prior to collapse. The extent and relative

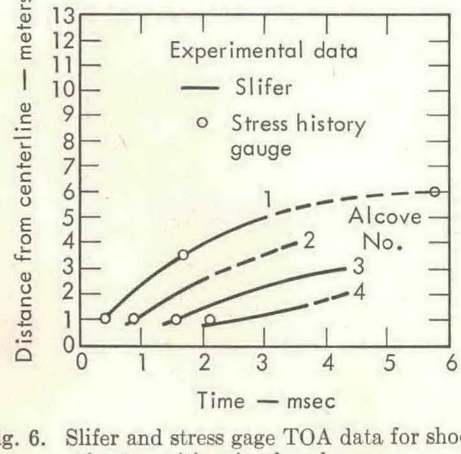

Fig. 6. Slifer and stress gage TOA data for shock-front position in the alcoves.

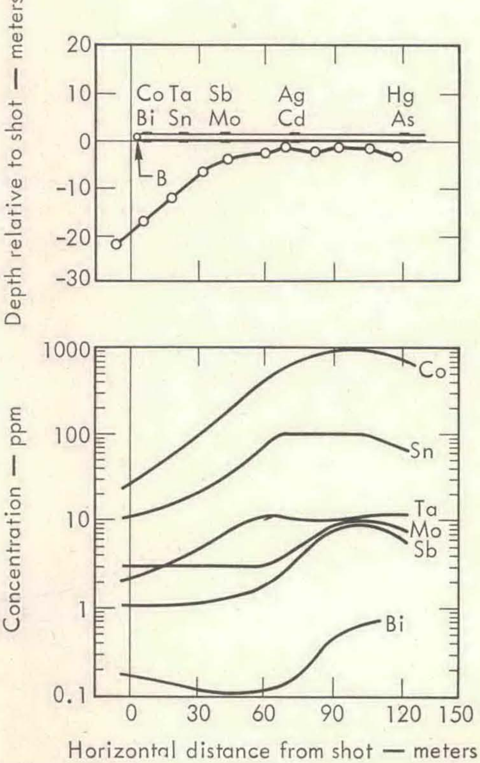

Fig. 7. The chemical tracers and their distribution. Upper figure: Location of chemical tracers in the tunnel and location of postshot samples. Lower figure: Analysis of the final tracer distribution.

TABLE 1. Chemical Tracers and Ablation Results

Layer	Tracer	Distance to Center of Tracer Section, meters	Thickness, cm	Inferred Minimum Ablation Thickness,† cm	Estimated Wall Mass Ablated, kg/m
A*	Co	6.1	10.2	>10.5	>134
B	Bi		0.3		
A*	Ta	21.4	5.1	>5.1	>4.4
B	Sn		2.5		
A*	Sb	39.6	2.5	>2.5	>1.6
B	Mo		1.3		
A*	Ag	70.2	1.3	<1.3	<0.9
B	Cd		1.3		
A*	Hg	119.0	0.3	<0.3	<1.0
B	As		5.1		

* Adjacent to the tunnel air.
† Inferred from Figure 7.

dimensions of the cavity at that time are illustrated in Figure 8 (L. A. Rogers, private communication, 1968). Further evidence of the nonspherical cavity growth is given by the asymmetric subsidence crater shown in Figure 9. The shot point was directly below the north edge of the concrete access-shaft pad, and the tunnel ran west, parallel to the cable tray. Thus the collapse crater extended at the surface from a few meters east of the shot point to approximately 60 meters along the tunnel.

3. Numerical Simulation

Numerical Codes

To consider simultaneously the time histories of the two shocks, down the tunnel and into the surrounding alluvium, the Tensor-Pufl [*Crowley and Barr*, 1971] code was developed. Tensor-Pufl is the combination of two finite-difference codes, Tensor [*Maenchen and Sack*, 1964] and Pufl [*Crowley*, 1967]. These codes, which increment the partial differential con-

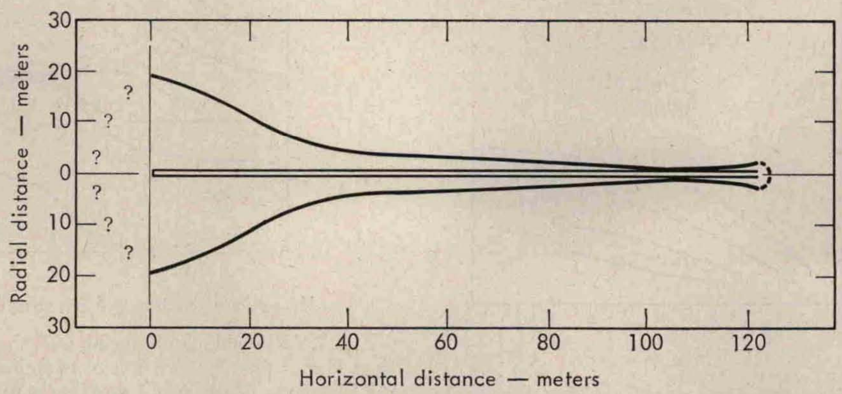

Fig. 8. Shape of the cavity before collapse, inferred from the postshot drilling data.

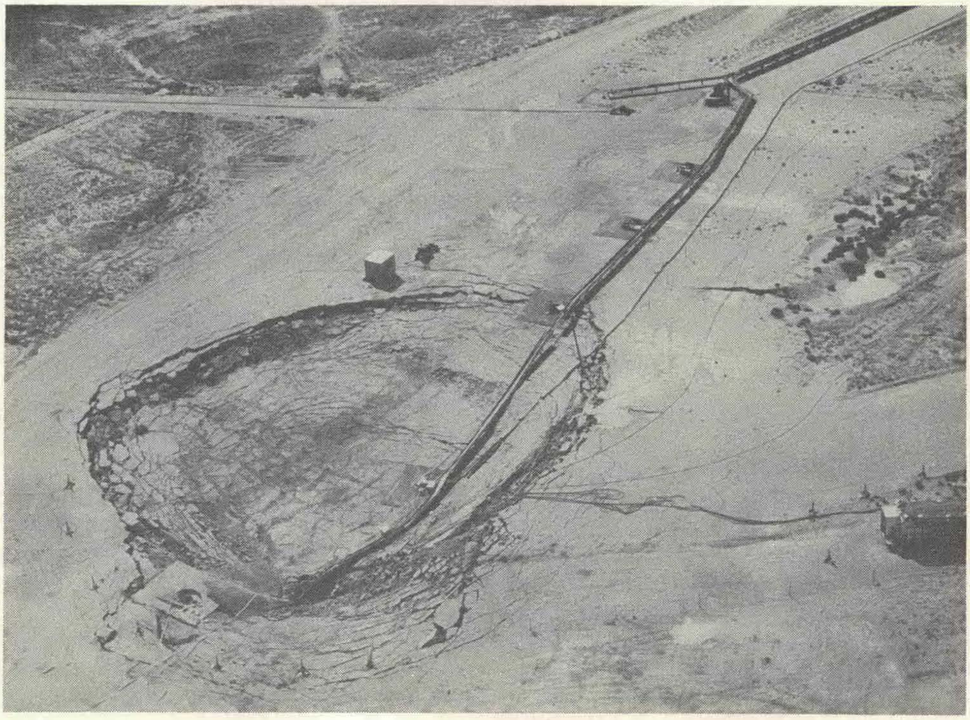

Fig. 9. Subsidence crater formed when the cavity collapsed. (View is to the southwest.) The square concrete block (left center of photo), now partly slumped into the crater, is the access-shaft pad. The shot point was directly below the north edge of the pad. The cable tray stretches from the pad along a path nine meters north of the tunnel. The crown block in the upper right corner lies directly above the end of the 122-meter tunnel. Along the cable tray are cable holes to the four instrument alcoves.

servation equations of continuum dynamics with respect to time, are based on the *von Neumann and Richtmyer* [1950] technique for the calculation of hydrodynamic shocks. The codes are discussed briefly below.

The Pufl conservation equations, which are shown in appendix A, are cast in 'pipe' geometry, where radial gradients are assumed to be negligible. Pufl zones are allowed to have mass sources or sinks; hence they are said to be 'almost Lagrangian.' To simulate the ablation process, auxiliary equations are used to calculate a heat sink and a mass source. In addition, an attempt is made to describe the radial turbulent diffusion of mass that enters from the walls of the pipe.

The Tensor equations are cast in the two-dimensional, cylindrically symmetric Lagrangian form. The equations consider the complete two-dimensional stress tensor composed of isotropic and deviatoric parts. Strain rates are calculated from the velocities, and stresses are obtained from the strains. General equations of state and other material properties such as the bulk and rigidity moduli may be used. Such effects as plastic yielding and fracture can also be considered. Tensor is used to simulate the alluvium off the axis of symmetry that surrounds the source region and the tunnel.

Tensor and Pufl are linked along their common boundary on each staggered time cycle in the CDC 6600 computer. They are run as two independent codes, with each supplying the other with the current boundary conditions. Pufl is entered and calculates pressures that it supplies to Tensor along the common boundary. Tensor is then entered and uses the pressures to calculate new radii, which are used by Pufl. Some details regarding this link are discussed by *Crowley and Barr* [1971].

Initial Conditions

The initial conditions used in Tensor-Pufl for the numerical simulation of Marvel are shown in Figure 10. Each Pufl zone extends between the axis of the tunnel and the inner wall of the tunnel. Initially, the Pufl zones are all 0.5 meter in radius. Axially, many Pufl zones are placed in each of the four material regions. Region 1 consists of alluvium and extends from −180 meters (minus infinity) to −0.75 meter. Region 2 is the source region that represents the homogeneous energy-source canister and consists of high-energy gas between −0.75 and +0.75 meter. Region 3 is the atmospheric air in the tunnel that extends from the end of the canister (zero point) to the end of the tunnel, +122 meters. Region 4 is again alluvium, from +122 to +300 meters (plus infinity). Tensor extends from −180 to +300 meters in the axial direction and from 0.5 to 180 meters (the surface) in the radial direction. All the two-dimensional array of cylindrical Tensor zones is alluvium.

The same material description for alluvium, which is based on an initial, average, in situ density (ρ_0) of approximately 1.7 g/cm^3, is used in Pufl and Tensor. During the early preshot operations, sound speeds were obtained in the alluvium between approximately 1000 and 1200 m/sec. Samples of the alluvium indicated a water content of approximately 5 wt%.

The pressure versus μ ($\mu = (\rho/\rho_0) - 1 =$ compression − 1) curves up to 40 kb shown in Figure 11*a* are provided by D. R. Stephens (private communication, 1969). Stephens obtained the curves by estimates based on his previously acquired data for alluvium [*Stephens et al.*, 1970].

Shock Hugoniot data for various initial density alluviums exist in the literature. We considered the P–μ data of *McQueen and Marsh* [1961], *Bass* [1966], *Shipman et al.* [1969], *Petersen et al.* [1969], and *Bass et al.* [1963]. When the compressions given in these reports are all adjusted for an initial density of 1.75 g/cm^3, the array of data shown in Figure 11*a* results. It is not clear whether this type of initial density adjustment is the best way to handle the data from different densities. However, it was felt that no one set of the data at one density was sufficient. Between 40 kb and 1 mb, we chose the smooth P–μ curve through the data points shown in Figure 11*a*.

To obtain higher pressure values, the P–μ curve was extrapolated. This extrapolation was

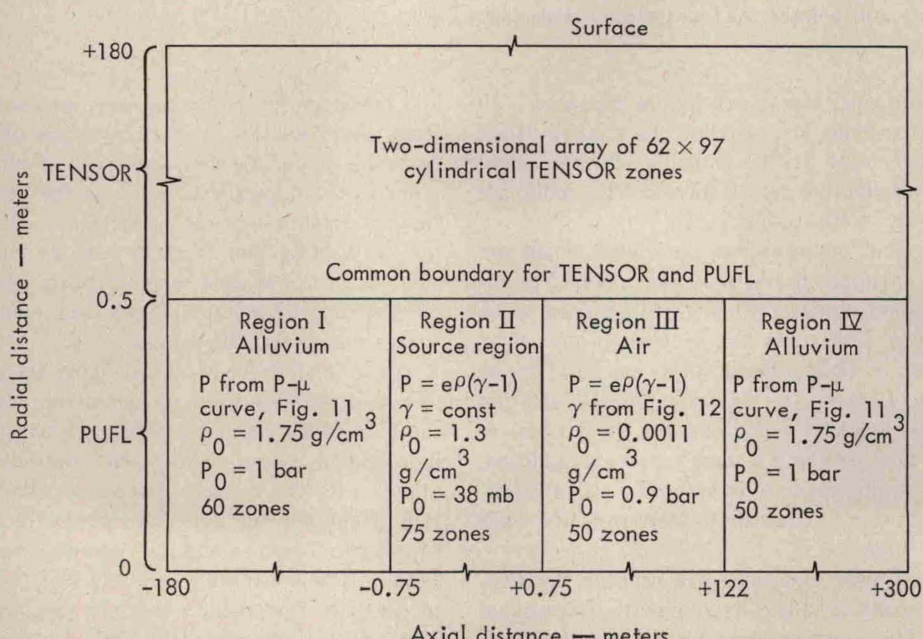

Fig. 10. Initial conditions used in Tensor-Pufl code for the numerical simulation of Marvel.

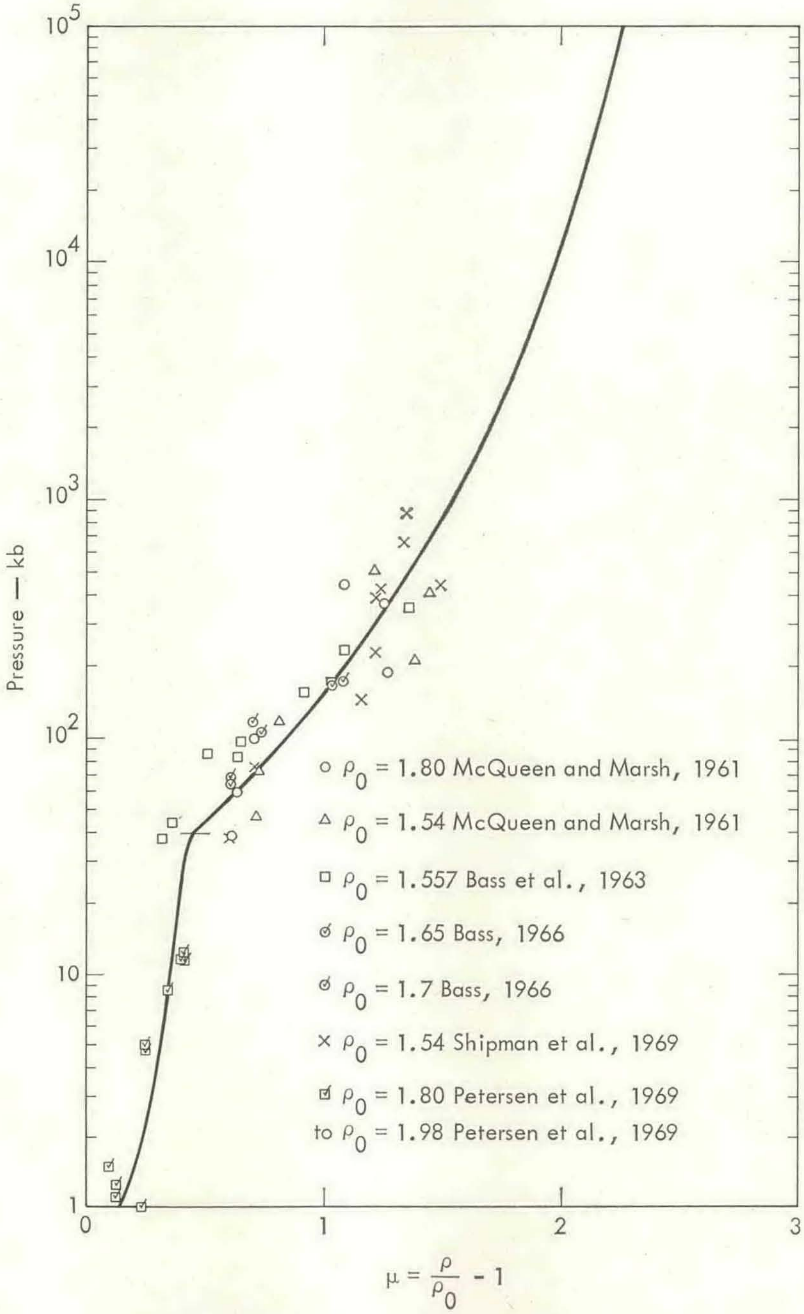

Fig. 11*a*. Consolidated and crushed P–μ curves for Marvel alluvium.

performed by continuing to increase the steepness of the P–μ curve slightly until, at 100 mb, $\mu = 2.25$. Preliminary calculations like those described here were performed, considering extrapolations to $\mu = 2.0$ and $\mu = 2.5$ at $P =$ 100 mb. At 100 μsec, the results of these two calculations were virtually identical with pressures in the cavity less than 1 mb. Thus, we feel that although the extrapolation used here ($\mu =$ 2.25 at $P = 100$ mb) is not based on experi-

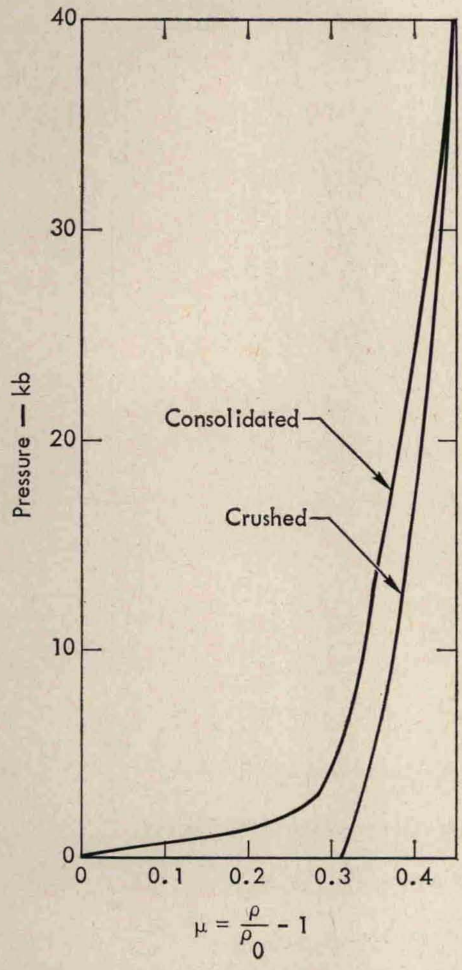

Fig. 11*b*. Details of lower-pressure portion of consolidated and crushed P–μ curves for Marvel alluvium.

mental data or theory, it may be adequate for the numerical simulation of the alluvium surrounding Marvel.

The initial slope of the loading P–μ curve indicates a bulk modulus of $k \approx 18$ kb. By use of $k = 18$ kb and the average measured sound speed of 1200 m/sec, a rigidity modulus of 6.5 kb is obtained. In order to minimize the rigidity of the material after it is considered to be crushed, a Poisson's ratio σ of 0.49 is assumed. This high ratio results in a lower rigidity modulus than that calculated for the consolidated material where $\sigma \approx 0.34$. An estimated yield curve for this very weak alluvium is shown in Figure 11*c*.

There was some concern that the density-matching grout that was used to backfill the drift would continue to release heat into the tunnel air after the access hole had been sealed. However, temperature sensors located in the grout registered nearly constant temperatures in the range of 100° ± 20°F for the three-week period before the shot date (Guido, personal communication, 1968). A 110°F temperature, 1100-meter altitude, an estimated 0.9-bar pressure, and a density of 1.1×10^{-3} g/cm³ were used as the initial conditions for the tunnel air.

An equation of state for air of the form $p = f(e)$, where pressure is a function of specific internal energy, is used in the calculations. This equation of state, which is shown in Figure 12, was obtained from air data at low energies [*Gilmore*, 1955] and shock relations at higher energies [*Fenter*, 1961]. Over the range of air densities encountered in Marvel ($\rho \approx 10^{-3}$ to 10^{-1} g/cm³), the pressure at a given specific energy is essentially independent of density; therefore the density dependence in the equation of state is neglected. An auxiliary equation of state, $T = f(e)$, which is shown in Figure 13, is used to obtain the air temperature for calculating the radiative heat flux. A table [*Bond et al.*, 1965] for Rosseland mean opacity, $K_R = f(T, \rho)$, is used for air.

The 2.2-kT yield of Marvel was designed to be initially distributed homogeneously in the source region of volume 1.2×10^6 cm³. This gave an energy per unit volume of (ϵ) 7.6×10^{13} ergs/cm³. The mass of the total source-region canister was approximately 1.6×10^6

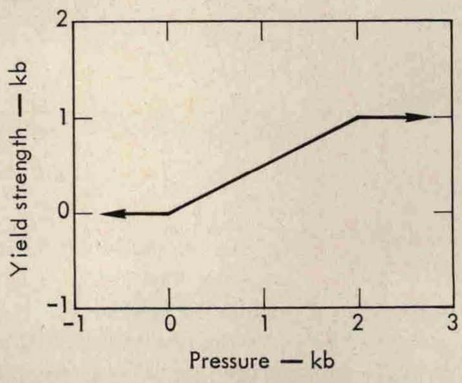

Fig. 11*c*. Estimated yield curve for the very weak Marvel alluvium.

grams, which indicates an initial density of $\rho = 1.3$ g/cm^3.

A variety of other materials was present in the source region, and an accurate equation of state for this region would be difficult to obtain. Therefore, to simulate the first 100 μsec of the source region, a constant value for γ was used and the pressure was calculated by $p = (\gamma - 1) \rho_e$. Two calculations with $\gamma = 1.5$ and 1.7 were performed, which gave nearly identical results at 100 μsec. The larger γ gave larger initial pressures, which acted to drive the shock down the tunnel faster. However, the larger pressure also acted to push out the walls of the cavity and tunnel at a more rapid rate, thereby relieving itself faster.

One-dimensional studies [*Butkovich*, 1967] indicate that within about 100 μsec, the ground shock from a 2.2-kT energy source can vaporize approximately 150 tons of alluvium. During this initial vaporization period, the various gases in the source are undoubtedly undergoing a very violent mixing. Within a few tens of microseconds, the source region contains a much

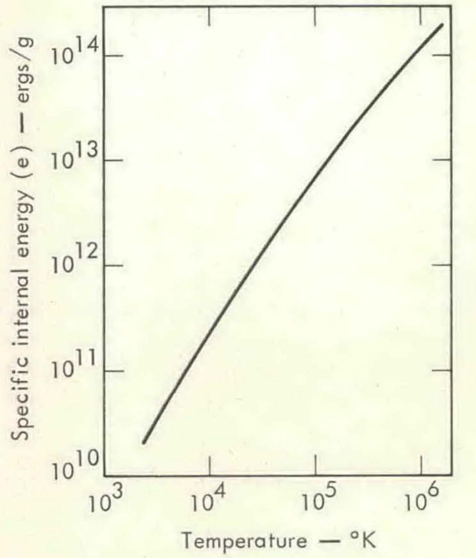

Fig. 13. Relationship used in Pufl to obtain temperature for a given specific internal energy.

larger mass of vaporized rock than the initial mass of source-region materials. The source region gas may then be represented by an equation of state for SiO_2 [*Butkovich*, 1967].

At 100 μsec, the two calculations with $\gamma =$ 1.5 and 1.7 indicate a radial vaporization contour that corresponds favorably to the 150 tons of vaporized mass indicated by the one-dimensional calculations. Because a considerable amount of vaporized rock gas is undoubtedly mixed with the source-region gases by 100 μsec, and because Tensor zones at present have no provision for varying their masses, these constant γ calculations were terminated at 100 μsec.

The Pufl and Tensor results at 100 μsec were combined, and the problem was rezoned to include the vaporized wall material in Pufl. This combination was performed by conservation of internal energies, momentums, and total masses of the vaporized material over each of about 75 axial sections of the problem. These rezoned conditions, which are shown in Figure 14, represent Marvel at 100 μsec. These conditions are used as the initial conditions for the remaining calculations.

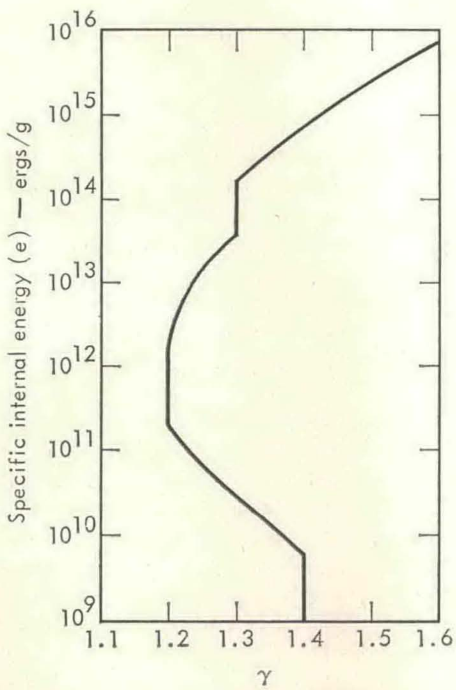

Fig. 12. Equation of state for air used by Pufl, specific internal energy as a function of γ: where $P = e(\gamma - 1)\rho$.

Calculations and Comparison with Data

The remaining calculations simulate the air shock and flow of gas down the tunnel. By comparison of various calculational results, the relative effects of radial expansion, heat transfer, and mass entrainment can be observed.

The first calculation, TP1, is an idealized case and may be used as a basis for comparison. In TP1, the friction, heat transfer, and mass addition terms were suppressed by setting $C_f = \sigma = C_H = 0$ and $\eta = \infty$ in equations A1–A6. As seen in Figure 15, air-shock velocity in this calculation is nearly unattenuated. The slight attenuation observed in this calculation is due to radial expansion of the cavity and tunnel walls, which reduces the pressure behind the shock. For comparison, the data from Figure 8 are also shown.

In the second calculation, TP2, the effect of heat transfer in attenuating the air shock is

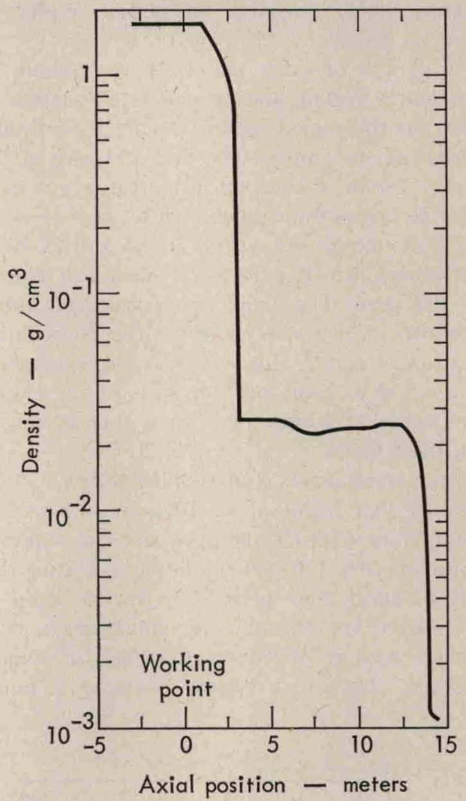

Fig. 14*b*.

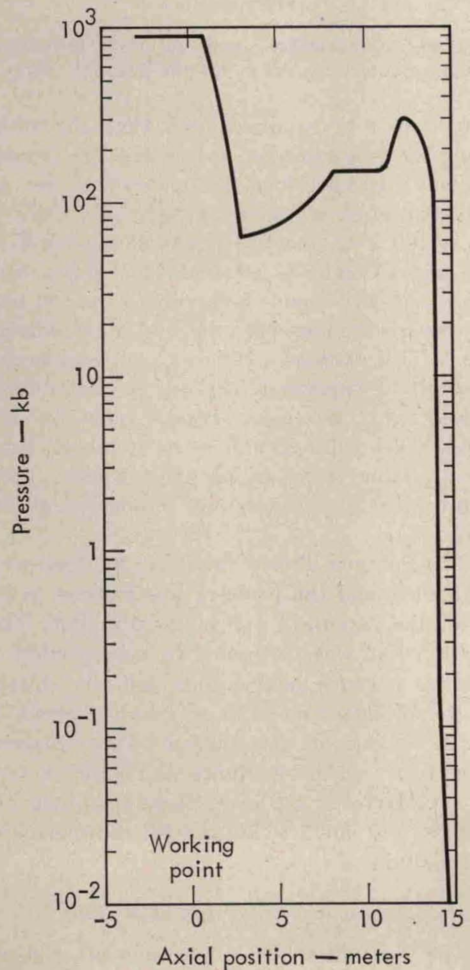

Fig. 14*a*.

investigated. As mentioned in section 1, the average offset in joining the sections of the tunnel was less than 0.3 cm. The 0.3-cm offsets were treated in the calculations as an average roughness, rather than as discontinuities. An estimate of 0.3 cm as the maximum surface roughness k_s gives a radius-to-surface-roughness ratio, $r/k_s = 170$. For turbulent flow with $r/k_s = 170$, a dimensionless coefficient of friction of $C_f/2 = 0.003$ is reasonable [*Schlichting*, 1960]. Invoking Reynolds's analogy (which assumes that the same mechanism induces the transfer of heat and momentum in turbulent flow), the dimensionless coefficient of heat transfer C_H is assumed to be $C_H = C_f/2 = 0.003$. These values are used for the dimensionless coefficients in the TP2 calculation. By setting the turbulent transpiration coefficient $\eta = \infty$ in TP2, mass addition is suppressed, and the effect of heat transfer may be examined.

Shock-arrival results from TP2 are shown in Figure 15, where it is seen that without mass addition, heat transfer does not account for the

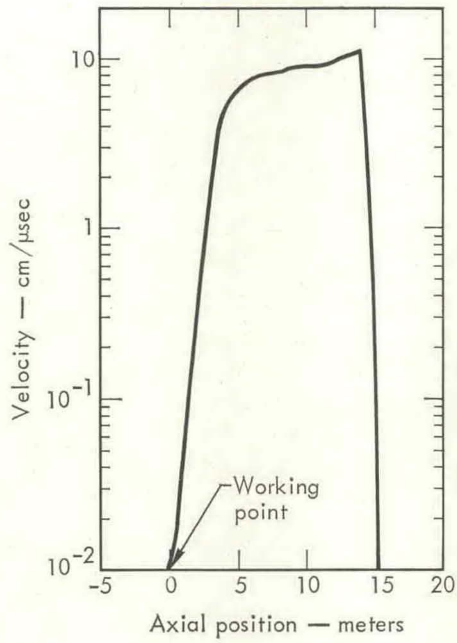

Fig. 14c.

Fig. 14 shows (a) pressure, (b) density, and (c) velocity conditions representing Marvel at 100 μsec. These conditions are used as initial conditions for the Tensor-Pufl calculations that simulate Marvel at later times.

experimentally observed attenuation of the air shock. In this calculation, approximately 5% of the initial energy was thermally transferred to the walls of the tunnel during the 1.85 msec it took the shock to travel 122 meters down the tube. This heat transfer was due almost exclusively to the turbulent convective heat flux. During this same interval, approximately 50% of the total initial energy was deposited in the surrounding alluvium by the radial ground shock.

Heat fluxes were also considered in the last two calculations, TP3 and TP4; in addition a mass flux was calculated by use of equations A5 and A6, with a turbulent transpiration coefficient of $\eta = 0.2$ [*Rose and Offenhartz*, 1959]. Figure 15 indicates that in comparison with the experimental data, too much attenuation is taking place too soon in the TP3 calculation. In TP3, the ablated mass is allowed to *instantaneously* enter and homogeneously mix within a total Pufl zone. Reasonable variations in the value of η did not substantially alter these TP3 results, which indicated too much attenuation was taking place too soon.

The TP4 calculation is exactly like TP3, except that an attempt was made to treat radial turbulent diffusion of ablated wall material (see appendix B), as opposed to its instantaneous mixing. Figure 15 indicates that the TP4 calculation more closely matches the experimental data at late times than does the TP2 calculation.

The TP3 and TP4 calculations indicate that mass addition was significant in attenuating the flow of high energy down the tunnel. Comparison of these calculations indicates that the time-dependent mixing prescription (TP4) is more realistic than the instantaneous mixing (TP3). However, the data indicate that even less mixing should be occurring at early times than is calculated by the TP4 calculation. This suggests a pressure dependence for the mixing rate that would require longer times for mixing when the pressure inside the pipe is high than when the pressure is low. Uncertainties in the time dependence of the radial turbulent diffusion of ablated material and the accuracy of the

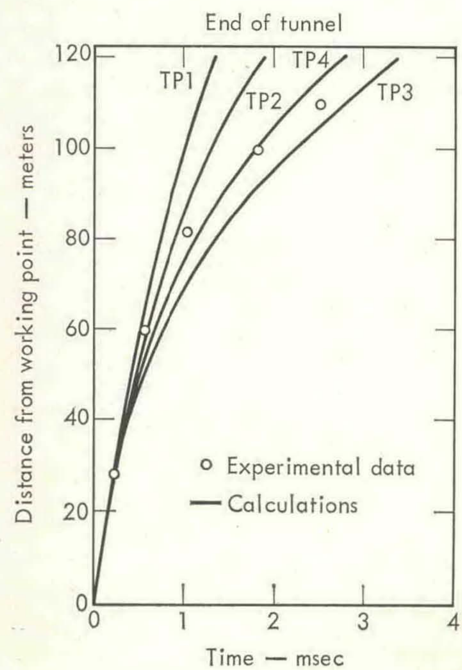

Fig. 15. Air-shock time of arrival showing experimental data and calculations that consider various physical phenomena.

ablation parameters limits the accuracy of shock prediction, particularly with one-dimensional calculation. In the following, the TP4 calculation is used for comparisons with the experimental data that was discussed in section 2.

Experimental shock TOA and the peak mean stress obtained from the stress-history gages that were located in the four alcoves, are given in Table 2. Table 2 also includes data from the cavity gas-pressure instrumentation in the fourth alcove. Results from the TP4 calculation are given in the last two columns of Table 2. At locations farther from the tunnel, the rise time of the pressure pulse is greater. Therefore, for consistency, the shock arrival time from the calculation is taken to be the time at which a pressure of at least 400 bars arrives at the specified location. The calculated peak pressures and their arrival times are given in the last column of Table 2.

The experimental results of the two free-field slifers and the four stress-history gage measurements are summarized in Figure 16. The two stress-history gages, which were located at a distance of 7.5 meters from the center line of the tunnel, saturated (>15 kb) at the time of arrival of the ground shock. The two gages located at 29.3 meters gave identical arrival times and similar peak pressures. Since the two gages were not saturated, their results are considered credible. Figure 16 also shows the calculated arrival times at specific positions for (1) pressures in excess of 100 bars, (2) pressures in excess of 400 bars, and (3) peak pressures. The magnitude of the peak pressure is indicated at each position. The TP4 calculation was terminated at 20 msec. However, when extrapolated, the calculation indicates the peak pressure and appears to be in agreement with the later time measurements (for both arrival and magnitude of the pressure) from the two gages located at 29.3 meters.

Generally, the TP4 calculation compares favorably with the experimental measurements from the alcoves (Table 2) and the 'free field' (Figure 16). This comparison in the surrounding media is sparse; a more complete comparison along with more data would have been desirable to put the calculations on a firmer basis. However, we believe that the existing comparison indicates that the calculations reasonably approximate the propagation of energy into the surrounding media and that the energy initially propagated from the canister into the alluvium approximately 50 times slower than it propagated down the air tunnel.

Figure 17 shows the position-time history of the contact surface (the rock–gas-air interface) from the TP4 calculation. After the air shock reaches the end of the tunnel, a reflected shock propagates back up the tunnel and interacts with the contact surface. This interaction impedes but does not reverse any appreciable mass flow down the tunnel. Although the cal-

TABLE 2. Stress History Gages and Cavity Pressure Gage Locations and Data

Gage No.	Alcove No.	Directed Toward	Distance from Centerline of Tunnel, meters	Distance from Working Point, meters	Experimental TOA, msec	Experimental $\hat{\sigma}_r$, kb	TP4 Calculational TOA,* msec	TP4 Calculational Peak Pressure,† kb
1	1	Tunnel	1.0	29.6	0.41	···‡	≤0.4	>30 at ~0.5
2		Tunnel	3.6	29.6	1.74	···‡	1.4	>5.0 at 1.8
3		Working point	6.0	29.4	5.75	0.5	4.0	~1 at 5.5
4	2	Tunnel	1.0	59.7	0.92	···‡	0.9	>15 at ~1.0
5	3	Tunnel	1.0	81.4	1.53	···§	1.4	>7 at 2.2
6	4	Tunnel	1.0	99.7	2.07	1.75	2.0	~3 at 3.2
C‖	4	Tunnel	0.5	100.0	2.1	1.8	1.8	>5.0 at 2.0

* Time of arrival for 400-bar pressure.
† Peak pressure at time of arrival (msec).
‡ Stress exceeded instrument range (15 kb).
§ No data; gage inoperable.
‖ Cavity gas-pressure instrumentation.

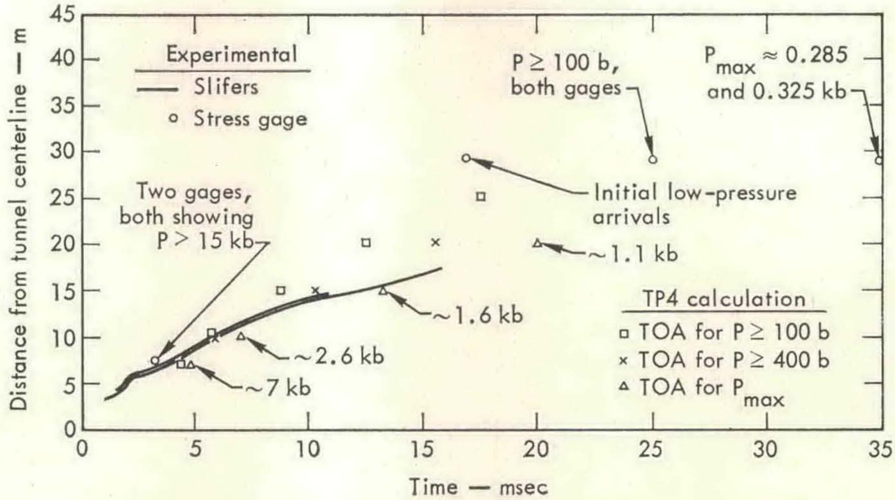

Fig. 16. Free-field measurements and calculated results for the vertical instrumentation hole.

culations indicate that some mass flow reverses direction at late times, the amount is small. Thus, most of the mass flow should end up at roughly the farthest position attained in the tunnel. The higher concentration of ablated chemical tracers near the end of the tunnel (see Figure 7) appears to be consistent with this result.

The TP4 calculation indicated that 4×10^{18} ergs of energy (approx. 5%) were transferred to the walls of the tunnel by heat transfer during the calculated 2.8-msec transit of the air shock down the tunnel. The calculation indicated that about ½ ton of wall material entered the flow during this interval. The mass addition rate exponentially decreases with time, and at 20 msec, approximately 1 ton of material had been entrained. Information from Table 1, which infers the amount of ablated material from the chemical tracers, can be used to estimate the amount of entrained wall material. Such rough estimates appear to be consistent with the 1-ton value calculated by TP4 for the entrained wall material at 20 msec.

At 20 msec, the TP4 calculation indicated that only a few per cent of the total energy was in kinetic energy. Most of this kinetic energy was located behind the shock front in the media (in Tensor) surrounding the tunnel, not in the tunnel gas (not in Pufl). In the calculation, approximately 17% of the energy was located at an axial position *beyond* 22 meters down the tunnel. Since no postshot drill holes were dug into the side of the cavity away from the tunnel, the total volume of the final cavity can only be estimated. Let us generously assume that the final main cavity is spherical with a 22-meter radius (the maximum radius indicated by postshot drill samples in Figure 7) and a volume of 4.5×10^4 m³. The volume of the final tunnel beyond 22 meters also can be obtained from the radii given in Figure 7; it is found to be about 6.7×10^3 m³. This is approximately 15% of the estimated main cavity volume. Thus, assuming that energy scales like the volume, both the calculations and the postshot drill samples indicate that at least ~15% of the energy was preferentially channeled down the tunnel.

CONCLUSIONS

By both calculation and experimental evidence, the initial shock traveled outward in the alluvium at about 2 m/msec. This is over 50 times slower than the initial 130-m/msec (Mach 380) velocity of the air shock. When the air shock reached the end of the tunnel (122 meters, ~3.5 msec), the shock in alluvium had traveled only 7.5 meters from the working point. The calculations and chemical-tracer analysis likewise agree that significant ablation occurred during the air-shock transit down the tunnel and that ablation has a primary effect in attenuating the air shock.

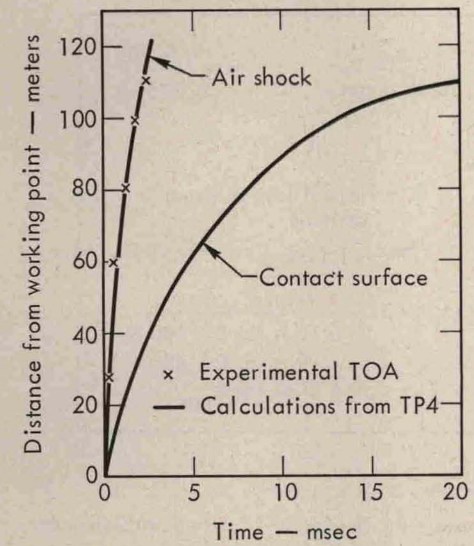

Fig. 17. Air-shock and contact-surface time of arrival.

The experimental and calculational results indicate that the emplacement of a nuclear explosive in a nonspherical initial geometry can result in significant nonspherical effects on the surrounding media. In Marvel, approximately 15% of the energy was channeled to distances beyond the main cavity radius. Energy was preferentially channeled down the tunnel, primarily because the velocity of the air shock in the tunnel was higher than the velocity of the alluvium shock.

If the shock in the surrounding media were to get ahead of the shock in the tunnel, the developed pressure gradient (existing between the 1 bar of tunnel air and the higher pressures behind the alluvium shock) would act to close the tunnel. A closure of the tunnel would inhibit the preferential flow of energy down the tunnel. Thus, the equation of state and the other properties of the materials immediately surrounding the energy source and the conditions in the tunnel can both be significant in determining the distribution of energy. However, we feel that, in Marvel, the large density difference between alluvium and air had the first-order effect on the initial shock velocities and the preferential distribution of energy. Since the densities of rocks are comparable to alluvium ($\rho \sim 2$ g/cm^3), it is felt that performing Marvel in a different media would not result in a significantly different distribution of energy. (Calculational parameter studies indicate that this is the case.) However, other effects that are more strongly material dependent, such as the extent of cracking, may significantly differ in different types of rock.

Whether significantly more energy could be channeled down a tunnel designed, for instance, twice as long as Marvel still remains to be answered.

Since flow in the tunnel would scale approximately as the ratio of the length to diameter, a tunnel of significantly smaller diameter would cause a faster attenuation. If this attenuation is fast enough, the shock in the surrounding material might overtake the tunnel shock in some designed instances. In such a case, the energy distribution could be significantly different.

The favorable agreement of the experimental data with the numerical simulation indicates that the Tensor-Pufl code can be used as a predictive technique for similar emplacements.

Marvel demonstrated the feasibility of hydrodynamically tailoring energy from a nuclear source. Economically tailoring nuclear energy for a particular application, such as mining or gas stimulation, is a fundamental goal of Plowshare.

APPENDIX A. PUFL CONSERVATION EQUATIONS

Pufl Equations

Conservation of mass.

$$\frac{\partial \rho}{\partial t} = \frac{1}{V}\left(-\rho \frac{\partial V}{\partial t} + \phi m' S\right) \qquad \text{(A1)}$$

$\phi m'S$ describes the change in density ρ due to the mass flux m'. The zone has a volume V and contacts the tunnel walls over a surface area. ϕ is defined in appendix B.

The momentum equation.

$$\frac{\partial u}{\partial t} = \frac{1}{m}\left[\phi m' S(u_w - u) - V\frac{\partial p}{\partial x} - T_w S\right] \qquad \text{(A2)}$$

The axial particle velocity u is modified by: the entering mass, whose axial velocity is u_w; the axial pressure gradient; and frictional stresses. $T_w = \frac{1}{2} C_f \rho u^2$, and C_f is the dimensionless coefficient of friction.

Conservation of energy.

$$\frac{\partial e}{\partial t} = \frac{1}{m}\left\{\phi m' S[(u - u_w)^2/2 + (e_w - e)] - p\frac{\partial V}{\partial t} + T_w S\,|u| + H'\right\} \qquad \text{(A3)}$$

The specific internal energy, e, is modified by: the entering mass, whose specific internal energy is e_w and whose velocity is u_w; volume changes; irreversible dissipative work done on a zone by the tunnel surface stresses; and (H' = energy/time) energy sources or sinks.

Equation of state. The functions can be any equation or table for each material present.

Heat transfer. The energy sink H' can be due to turbulent convective heat flux q_c and a radiative heat flux q_r. These heat fluxes transfer energy through the surface area S of the zone that is in contact with the tunnel walls. The heat fluxes are calculated by *Bond, Watson and Welch* [1965], *Schlichting* [1960], and *Rose and Offenhartz* [1959]

$$H' = -S(q_c + q_r) = -S\left(\frac{C_H\gamma p u}{\gamma - 1} + \frac{4\sigma T^4}{3\rho K_R(R/2)}\right) \qquad \text{(A4)}$$

where p is pressure, u is particle velocity, γ is the ratio of specific heats, C_H is the dimensionless coefficient of turbulent heat transfer (the Stanton number), σ is the Stefan-Boltzmann constant, T is the temperature of the gas, and K_R is the Rosseland mean opacity, which is obtained from a temperature- and density-dependent table.

Ablation mass flux. The mass flux that enters the flow, m', is related to H' by

$$m' = \frac{q_c + q_r}{q^*} = -\frac{H'}{Sq^*} \qquad \text{(A5)}$$

where

$$q^* = E_v + \eta h \qquad \text{(A6)}$$

and q^* is the energy required to ablate a unit mass of wall material, E_v is the total specific heat required to vaporize wall material ($E_v \approx 10^{11}$ ergs/g for rock), h is the specific total enthalpy of the gas flow in the tunnel, and η is the turbulent transpiration coefficient ($\eta \approx 0.2$ for rock) [*Rose and Offenhartz*, 1959].

APPENDIX B. TURBULENT DIFFUSION OF ABLATED WALL MASS

A set of hypothetical Eulerian regions are considered axially along the walls of the tunnel. When ablation starts in one of these regions, the time T_s is noted. Then, at any later time T the time interval $T_i = T - T_s$ can be calculated. T_i is the time during which turbulent diffusion has carried gas a distance Y [*Schlichting*, 1960], measured *from* the wall, where

$$Y = R\left\{1 - \left[1 - \frac{T_i u (C_f/2)^{1/2}}{2R}\right]^2\right\} = R[1 - (1 - \beta)]^2 \qquad \text{(B1)}$$

and R is pipe radius, u is free stream velocity, $C_f/2$ is the dimensionless coefficient of friction, and all quantities are averaged over the Pufl zones within a hypothetical Eulerian wall region.

Until the mass leaving the wall diffuses to the center of the pipe, the calculated ablation mass flux has only a partial effect on the total Pufl zone. It is assumed that this partial effect is proportional to the volume of the Pufl zone that the entering mass occupies at any time. The ratio of the volume occupied by the entering mass to the volume of the inside of the pipe is denoted by ϕ and calculated for each Eulerian region by

$$\phi = 1 - (R - Y)^2/R^2 = 1 - (1 - \beta)^4 \qquad \text{(B2)}$$

The ablation mass fluxes, calculated for each Lagrangian Pufl zone by equation A5, are multiplied by the appropriate ϕ, depending on the Eulerian region in which the almost-Lagrangian Pufl zone is located.

Acknowledgments. A complete list of the people who contributed to Marvel would easily extend to over a hundred names, and such a list is virtually impossible to compile. Each person mentioned below relied on many others, and it was this combined effort of many individuals that made Marvel possible. L. A. Rogers, project physicist, and R. S. Guido, project engineer, led the program. P. D. Compton worked extensively with us on both the design and instrumentation; G. T. Pelsor, S. Sack, and F. C. Cook, on design of the homogeneous source region; F. E. Locke, on chemical tracers; B. C. Maranville, D. R. Garner, and J. B. Currey, on engineering and emplacement of instrumentation; and J. N. Vierra and J. B. Carson, on electronic recording. Field operations and mining were performed by the Reynolds

Electric and Engineering Company. The miners working on Marvel contributed through many efforts not normally required; without their careful and willing help, the Marvel design could not have been implemented. H. G. Hicks was responsible for the postshot drilling and data analysis. L. K. Barr, E. A. Reed, and J. G. Shaw worked with the code development and numerical calculations. C. L. Myers typed many of our papers for Marvel.

The work was performed under the auspices of the U.S. Atomic Energy Commission.

REFERENCES

Bass, R. C., Additional Hugoniot data for geologic material, *Sandia Corp. Rep. SC-RR-66-548*, 1966.

Bass, R. C., H. L. Hawk, and A. J. Chabai, *Sandia Corp. Rep. SC-RR-4903*, 1963.

Bond, J. W., Jr., K. M. Watson, and J. A. Welch, Jr., *Atomic Theory of Gas Dynamics*, 518 pp., Addison-Wesley, Reading, Mass., 1965.

Butkovich, T. R., Calculation of the shock wave from an underground nuclear explosion in granite, *J. Geophys. Res., 70,* 885–892, 1965.

Butkovich, T. R., The gas equation of state for natural materials, *Lawrence Radiat. Lab. Rep. UCRL-14729,* 1967.

Cherry, J. T., Computer calculations of explosion-produced craters, *Int. J. Rock Mech. Mining Sci., 4,* 1–22, 1967.

Crowley, B. K., PUFL, an 'almost-Lagrangian' gasdynamic calculation for pipe flows with mass entrainment, *J. Comp. Phys., 2,* 61–86, 1967.

Crowley, B. K., and L. K. Barr, TENSOR-PUFL: Boundary condition linked codes, *J. Comput. Phys., 7,* 167–171, 1971.

Fenter, F. W., The thermodynamic properties of high-temperature air, *Chance Vought Res. Center Rep. RE-1R-14,* 1961.

Gilmore, F. P., Equilibrium composition of thermodynamic properties of air to 24,000°K, *Rand Corp. Rep. RM-1543,* 1955.

Glenn, H. D., and B. K. Crowley, Marvel—Nuclear driven shock-tube experiment, *J. Appl. Phys., 41,* 689–697, 1970.

Heusinkveld, M., and F. Holzer, A method of continuous shock front position measurement, *Rev. Sci. Instrum., 35,* 1105–1107, 1964.

McQueen, R. G., and S. P. March, Equation of state of Nevada alluvium, *Los Alamos Sci. Lab. Rep. LAMS-2760,* 1961.

Maenchen, G., and S. Sack, The Tensor code, in *Methods of Computational Physics,* vol. 3, p. 181, Academic, New York, 1964.

Petersen, C. F., W. J. Murri, and R. W. Gates, Dynamic properties of rocks, *Def. At. Support Agency Rep. 2298, SRI-PGU-6273,* 1969.

Rodean, H. C., Understanding and constructively using the effects of underground nuclear explosions, *Rev. Geophys., 6,* 401–445, 1968.

Rogers, L. A., Free-field motion near a nuclear explosion in salt: Project Salmon, *J. Geophys. Res., 71,* 3415–3426, 1966.

Rose, P. H., and E. Offenhartz, Ablation measurements in turbulent flow, *Avco-Everett Res. Lab. Rep. AVCO-PR-114,* 1959.

Schlichting, H., *Boundary Layer Theory,* McGraw-Hill, pp. 457–557, New York, 1960.

Shipmen, F. H., W. M. Isbell, and A. H. Jones, High-pressure Hugoniot measurements for several Nevada Test Site rocks, *Def. At. Support Agency Rep. 2214, MSL 68-15,* 1969.

Stephens, D. R., E. M. Lilley, and H. Louis, Pressure-volume equation of state of consolidated and fractured rocks to 40 kbar, *Int. J Rock Mech. Mining Sci., 7,* 275–296, 1970.

von Neumann, J., and R. D. Richtmyer, A method for the numerical calculation of hydrodynamic shock, *J. Appl. Phys., 21,* 232–237, 1950.

(Received October 26, 1970;
revised February 3, 1971.)